



OPEN

## Study on the effect of size on InGaN red micro-LEDs

Ray-Hua Horng<sup>1</sup>✉, Chun-Xin Ye<sup>2</sup>, Po-Wei Chen<sup>2</sup>, Daisuke Iida<sup>3</sup>, Kazuhiro Ohkawa<sup>3</sup>, Yuh-Renn Wu<sup>4</sup> & Dong-Sing Wu<sup>2,5</sup>✉

In this research, five sizes ( $100 \times 100$ ,  $75 \times 75$ ,  $50 \times 50$ ,  $25 \times 25$ ,  $10 \times 10 \mu\text{m}^2$ ) of InGaN red micro-light emitting diode (LED) dies are produced using laser-based direct writing and maskless technology. It is observed that with increasing injection current, the smaller the size of the micro-LED, the more obvious the blue shift of the emission wavelength. When the injection current is increased from 0.1 to 1 mA, the emission wavelength of the  $10 \times 10 \mu\text{m}^2$  micro-LED is shifted from 617.15 to 576.87 nm. The obvious blue shift is attributed to the stress release and high current density injection. Moreover, the output power density is very similar for smaller chip micro-LEDs at the same injection current density. This behavior is different from AlGaInP micro-LEDs. The sidewall defect is more easily repaired by passivation, which is similar to the behavior of blue micro-LEDs. The results indicate that the red InGaN epilayer structure provides an opportunity to realize the full color LEDs fabricated by GaN-based LEDs.

Solid-state light emitting diodes (LEDs) have the advantages of self-luminescence, high brightness, and good stability. Compared with organic LEDs (OLEDs), they offer higher resolution, contrast, and a longer life, thus gaining immense popularity<sup>1,2</sup>. To achieve high resolution, the size of the micro-LEDs ( $\mu$ -LEDs) must be reduced so that more pixels can be placed in a unit display area. Up to now, blue GaN-based and red AlGaInP-based LEDs have been fabricated into  $\mu$ -LEDs with dimensions smaller than  $100 \times 100 \mu\text{m}^2$ . Chip size is found to affect the performance of  $\mu$ -LEDs. The decrease in the external quantum efficiency (EQE) of  $\mu$ -LEDs with size has been widely studied and reported on<sup>3,4</sup>. The increasing ratio of surface area to volume for the device results in various non-radiative losses at the device edge. The defects at the sidewall are caused by an inductively coupled plasma (ICP) etching process, which led to the increased Shockley–Read–Hall (SRH) non-radiative recombination. These defects result in lower EQE of  $\mu$ -LEDs with smaller diameter<sup>4,5</sup>. Although sidewall passivation can improve the injection current efficiency and EQE, AlGaInP  $\mu$ -LEDs typically suffer from much stronger size-dependent efficiency reduction owing to their high surface recombination velocities, longer carrier diffusion lengths<sup>6,7</sup>, and limited improvements through sidewall passivation<sup>8</sup>. Recently, InGaN-based red  $\mu$ -LEDs have been successfully grown by metal–organic chemical vapor deposition (MOCVD) on  $\text{Ga}_2\text{O}_3$ , sapphire, and Si substrates<sup>9–11</sup>. Most studies on the red light InGaN epilayer focused on the characteristics of its epitaxial technology, structure, and emission wavelength. To increase the optical power output, the thickness of the undoped GaN layer and the n-GaN layer is increased, which results in the emission wavelength and EQE of the red InGaN LED (@20 mA) to be 633 nm and 1.6%, respectively<sup>12,13</sup>. Although ultra-small ( $< 10 \mu\text{m}$ ) 632 nm red InGaN  $\mu$ -LEDs with useful on-wafer EQE ( $> 0.2\%$ ) has been published<sup>14</sup>, the chip size effect on the InGaN  $\mu$ -LED's performance has not been studied. In this work, the red light InGaN structure was used to fabricate  $\mu$ -LEDs with dimensions of  $100 \times 100$ ,  $75 \times 75$ ,  $50 \times 50$ ,  $25 \times 25$ , and  $10 \times 10 \mu\text{m}^2$  for the chip size effect study. The optoelectronic characteristics were analyzed through the current and voltage relation, electroluminescence (EL) spectra, and light output power density as a function of the chip size of  $\mu$ -LEDs.

### Results and discussion

Figure 1a shows the forward current density–voltage ( $J$ – $V$ ) characteristic for all chips. The turn-on voltage of  $\mu$ -LEDs from large to small chips is 3.05, 3.06, 3.04, 3.13, and 2.99 V, respectively, for an injected current density of approximately  $10 \text{ A/cm}^2$  (corresponding 1 mA for  $10 \times 10 \mu\text{m}^2$ ). At 4 V, the current density of  $\mu$ -LEDs from

<sup>1</sup>Institute of Electronics, National Yang Ming Chiao Tung University, Hsinchu 30010, Taiwan, ROC. <sup>2</sup>Department of Materials Science and Engineering, National Chung Hsing University, Taichung 40227, Taiwan, ROC. <sup>3</sup>Computer, Electrical and Mathematical Sciences and Engineering (CEMSE) Division, King Abdullah University of Science and Technology (KAUST), Thuwal 23955-6900, Saudi Arabia. <sup>4</sup>Graduate Institute of Photonics and Optoelectronics, National Taiwan University, Taipei 10617, Taiwan, ROC. <sup>5</sup>Department of Applied Materials and Optoelectronic Engineering, National Chi Nan University, Nantou 54561, Taiwan, ROC. ✉email: rhh@nctu.edu.tw; dsw@ncnu.edu.tw

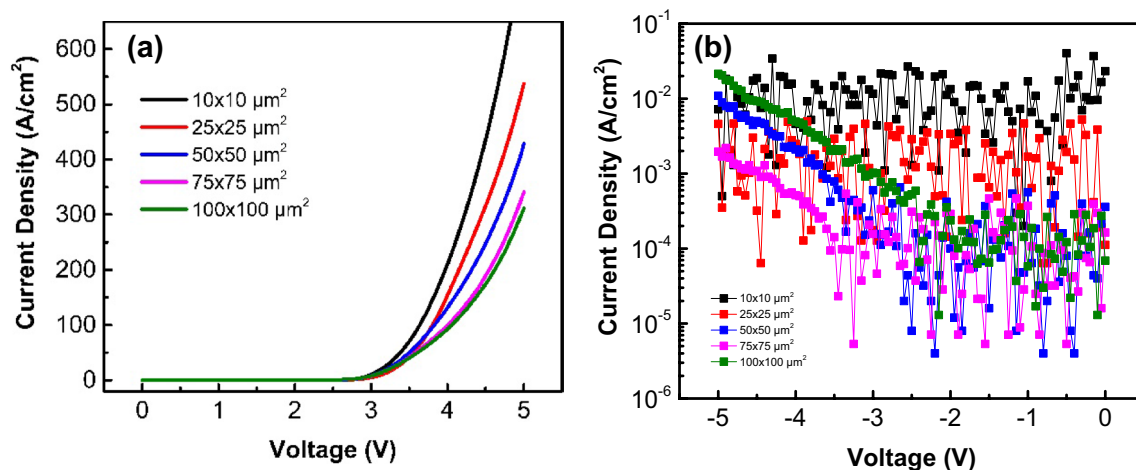


**Figure 1.** (a) Forward current density–voltage ( $J$ – $V$ ) characteristic for all chips and (b) leakage behavior for  $\mu$ -LEDs with different sizes.

$\mu$ -LED dimensions ( $\mu\text{m}^2$ )	Mesa area ( $\mu\text{m}^2$ )	Sidewall area ( $\mu\text{m}^2$ )* <sup>a</sup>	Sidewall surface ratio* <sup>b</sup>
10 × 10	100	20.6	0.171
25 × 25	625	51.5	0.076
50 × 50	2500	103	0.040
75 × 75	5625	154.5	0.027
100 × 100	10,000	206	0.020

**Table 1.** Comparison of total surface area and side wall surface area of different sizes of  $\mu$ -LEDs. \*<sup>a</sup>Mesa depth = 515 nm. \*<sup>b</sup>Sidewall surface ratio = sidewall area/total surface area.

large to small chips is 92.7, 99.8, 131, 154, and 210 A/cm<sup>2</sup>, respectively. Clearly, the current density increases as the size decreases. When the  $\mu$ -LED light-emitting area is reduced, the volume and resistivity also reduce. Under the same current density, the forward voltage decreases as the chip size is reduced. Moreover, under the same bias voltage, a small-sized  $\mu$ -LED will have a larger current density.

The main issue is the leakage current for  $\mu$ -LEDs. The leakage behavior for  $\mu$ -LEDs with different sizes is shown in Fig. 1b. It was previously reported that the leakage current is related to the sidewall<sup>5</sup>. The relationship between the sidewall surface area and the total surface area of the  $\mu$ -LED is shown in Table 1. First, the same number of defects per unit sidewall surface area is assumed. As the size is reduced, the sidewall surface area and the number of sidewall defects also decreases; nevertheless, the ratio of sidewall surface area to the total surface area increases. This suggests that the number of defects per unit total area increases and the effect of sidewall defects also increases for small-sized  $\mu$ -LEDs.

It is found that the leakage current density increases as the size decreases under a reverse voltage less than 3 V. The leakage density of  $\mu$ -LEDs with the smallest dimensions was the highest. This indicates that the leakage current could be caused by sidewall defects. Moreover, it could also be caused the largest electric field from the electrode to the edge (shortest distance = 3.5  $\mu\text{m}$  for  $\mu$ -LED with 10 × 10  $\mu\text{m}^2$ ) as the reverse voltage less than 3 V. The electric field (@ -3 V) from the electrode to the edge was  $2.3 \times 10^3$ ,  $4.0 \times 10^3$ ,  $6.0 \times 10^3$ ,  $4.8 \times 10^3$ , and  $8.5 \times 10^3$  V/cm of  $\mu$ -LEDs from large to small chip size. It is worthy to mention that the leakage current density of  $\mu$ -LEDs from large to small chip size is  $2.14 \times 10^{-2}$ ,  $1.96 \times 10^{-3}$ ,  $1.09 \times 10^{-2}$ ,  $4.59 \times 10^{-3}$ , and  $7.2 \times 10^{-3}$  A/cm<sup>2</sup> for a reverse voltage of 5 V. As the reverse voltage increases, the leakage increases more obviously for larger chip size, especial for the  $\mu$ -LED with 100 × 100  $\mu\text{m}^2$ . This suggests that not only is the leakage current relative to the sidewall passivation and the lateral electric field, the defects distributed on the surface could also affect the leakage current density. The large-sized LEDs cover a large area. It causes the leakage current density of large-sized  $\mu$ -LEDs (100 × 100, 75 × 75, and 50 × 50  $\mu\text{m}^2$ ) to increase and to be close to, and even higher than, those of small-sized  $\mu$ -LEDs (20 × 20 and 10 × 10  $\mu\text{m}^2$ ). Because there exist many defects in the InGaN epilayers<sup>12,15</sup>, this could also cover more defects. This causes leakage as the reverse bias increases.

Figure 2a shows the optical output power density as a function of the injection current density. As the injected current increases, the optical output power increases for all the chips. It was found that there were two groups. One group is for the larger chips with areas of 100 × 100 and 75 × 75  $\mu\text{m}^2$ . The other group is for chip sizes with areas 50 × 50, 25 × 25, and 10 × 10  $\mu\text{m}^2$ . If the output power density is affected by the sidewall, the smallest chip  $\mu$ -LEDs should show the lowest power density. As shown in Table 1, the  $\mu$ -LED with an area of 10 × 10  $\mu\text{m}^2$  presents the largest sidewall surface ratio. If leakage is the main issue affecting the output power, the short distance between the p-electrode and the edge could be an important parameter. As shown in Fig. 5b, the short distance

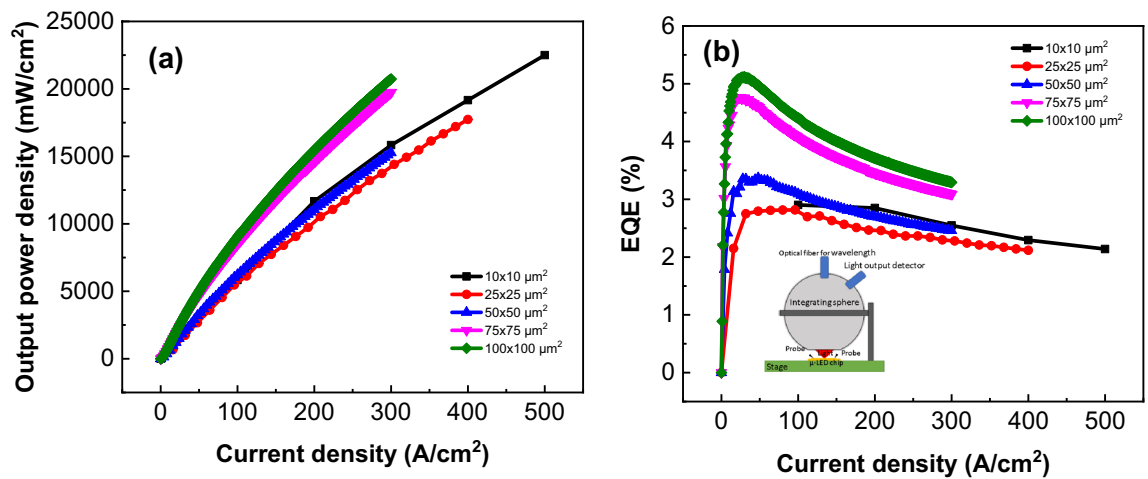


**Figure 2.** (a) Optical output power densities and (b) EQE as function of injection current densities for all chip size  $\mu$ -LEDs. The setup of on-wafer EQE measurement shown in the inset of (b).

between the p-electrode and the edge is 12.5, 7.5, 5, 6.3, and 3.5  $\mu\text{m}$  for all chips and sizes in order. Moreover, at the same injection current density, the distance from the electrode to the edge is only 3.5  $\mu\text{m}$  for the smallest size chip. Considering the sidewall surface ratio and the distance to the edge, the smallest dimension  $\mu$ -LEDs would obtain the smallest output power density. However, for the  $10 \times 10 \mu\text{m}^2$   $\mu$ -LEDs shown in Fig. 2a, this does not produce the smallest output power density. Evidently, the passivation layer provides the sidewall protection from leakage. This causes the output power density to be very similar for smaller  $\mu$ -LEDs. This is different from the behavior of AlGaInP  $\mu$ -LEDs. Obviously, the sidewall defect is more easily repaired by passivation. This is similar to the behavior of blue  $\mu$ -LEDs. Larger chips ( $100 \times 100$  and  $75 \times 75 \mu\text{m}^2$ ) show higher output power density than smaller chips ( $50 \times 50$ ,  $25 \times 25$  and  $10 \times 10 \mu\text{m}^2$ ). This might be attributed from the fact that larger chips contribute to light reflection from the bottom.

Figure 2b shows the EQE as a function of injection current densities. The maximum EQE is 5.11, 4.75, 3.36, 2.81 and 2.91% corresponding to the chip size in order. Note that the maximum EQE occurs at almost the same current density, except the  $10 \times 10 \mu\text{m}^2$  chip. It is due to the output power is too small to measure as the low injecting current density for the  $10 \times 10 \mu\text{m}^2$  chip. Moreover, it has been reported that the maximum EQE is shifted to higher current densities as the chip size decreases for the AlGaInP  $\mu$ -LEDs. The shift of maximum EQE was related to leakage current and/or an increased Shockley–Read–Hall (SRH) non-radiative recombination at sidewall defects in the smaller geometries<sup>14,16</sup>, although the sidewall had been passivated. However, the phenomena does not be observed in the red InGaN  $\mu$ -LEDs. The obtained results were consistent with that in Fig. 2a, i.e., the sidewall defects can be repaired by passivation. On the other hand, the droop behavior was more alleviative for the small size  $\mu$ -LEDs. It could be due to the fact that there exist more defects or phase separation for the  $\mu$ -LEDs with larger size. These defects could trap the carriers and reduce the EQE. As concerning this point, it has been demonstrated by TEM measurement<sup>12</sup>. Furthermore, it was found that the EQE of the  $\mu$ -LEDs with  $10 \times 10 \mu\text{m}^2$  was higher than those of  $\mu$ -LED with  $25 \times 25 \mu\text{m}^2$  and  $50 \times 50 \mu\text{m}^2$ . For smaller mesa size, the contribution of light coupled through the mesa edge compared to the surface becomes larger. This causes an increase of the external quantum efficiency (EQE) by light extraction. It was worthy to mention although the epilayer structure was the same with Refs.<sup>12,14</sup>, the obtained EQE in this work is higher than those of Refs.<sup>12,14</sup>. It could be due to the different device fabrication parameters, geometry of the metallic contacts, mesa outline and chip sizes.

Figure 3 shows the wavelength of  $\mu$ -LEDs with different sizes as a function of current. The wavelength decreases as the current increases, exhibiting blue shift behavior. It is well known that the blue shift phenomenon in blue and green InGaN-based LEDs grown on c-plane sapphire due to the InGaN QWs is caused by the screening of the piezoelectric field and band filling of the localized state. The same behavior is also exhibited in the InGaN  $\mu$ -LEDs with high In composition<sup>13–18</sup>. Moreover, the wavelength decreases as the chip size is reduced. This can be attributed to several possible reasons. The first is stress release in small dimensional LEDs. Second, smaller-sized chips have larger current densities, which leads to screening of QCSE and also band filling effects. To verify this, we applied a 1D Poisson and drift–diffusion solver (1D-DDCC) developed by Prof. Wu's lab in NTU<sup>19,20</sup>. With the same structure as shown in Fig. 1, we can simulate the band bending, confined energy, and emission spectrum at different densities. Figure 3a indicates that at a driving current of 0.1 mA, the emission wavelengths from large to small are 663.78, 651.76, 645.51, 639.97, and 617.15 nm in order. Furthermore, the emission wavelengths from large to small are 636.24, 617.55, 612.98, 605.87, and 576.87 nm in order as a driving current increasing to 1 mA. Obviously, the  $\mu$ -LED with  $10 \times 10 \mu\text{m}^2$  did not emit the red color wavelength as the injection current was higher than 0.1 mA. The current density versus chip size as shown in Fig. 3c reveals a trend with small variation for different chip sizes. To understand the mechanism for this large range of blue shift, 1D simulation was performed for different current densities. It shows that blue shift from 660 nm ( $0.1 \text{ A/cm}^2$ ) to 590 nm ( $1 \text{ kA/cm}^2$ ) is possible. This blue shift is caused by (1) screening of QCSE and (2) band filling effects. Our calculations show that blue shift from 660 to 620 nm is mainly due to the screening of QCSE. After  $10 \text{ A/cm}^2$ , the band filling effect becomes stronger and the emission spectrum widens as shown in Fig. 3d. The

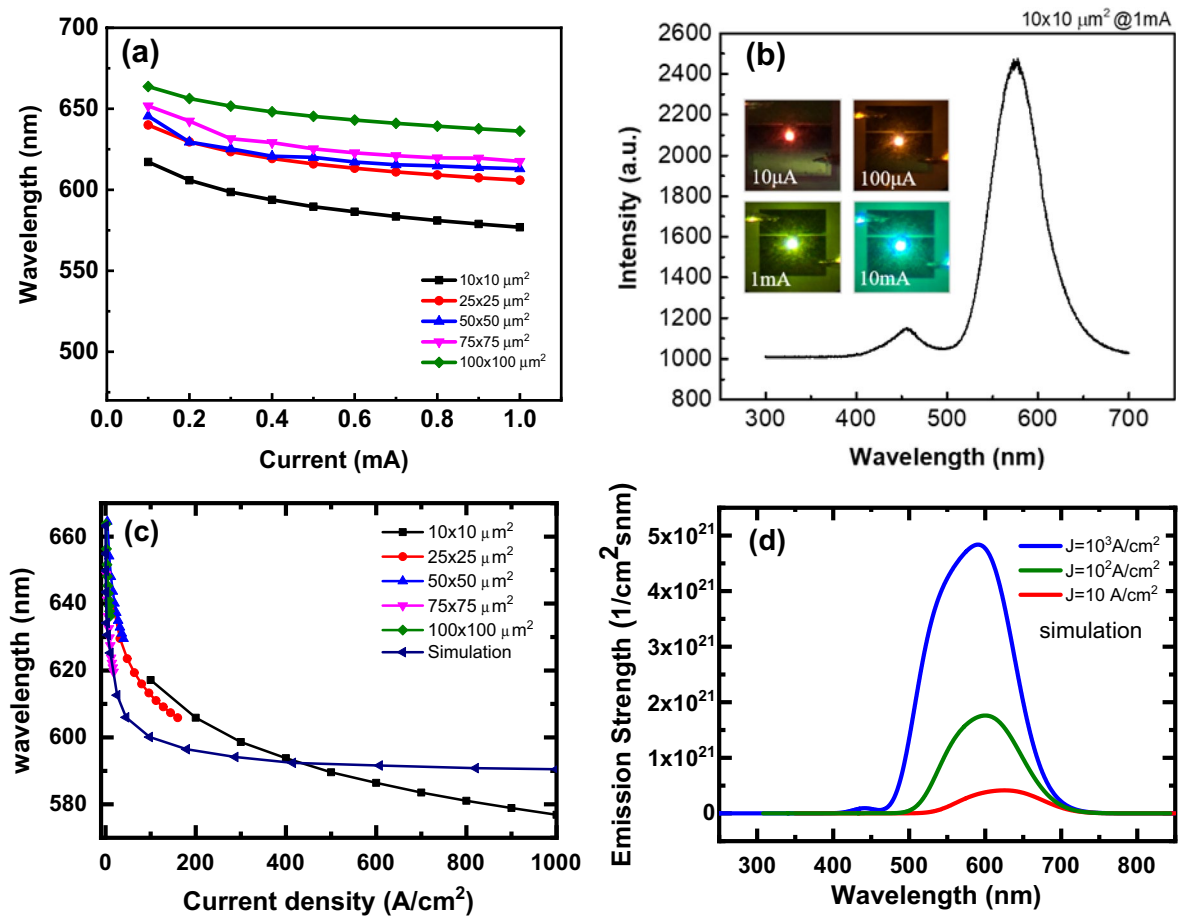


**Figure 3.** (a) Wavelength as a function of current of red  $\mu$ -LEDs of different sizes under driving currents from 0.1 to 1 mA and (b) EL spectrum for the  $\mu$ -LED with area  $10 \times 10 \mu\text{m}^2$  for an injection current of 1 mA. (c) Wavelength shift versus current density for both experimental and simulation results and (d) Simulation emission spectra under different current density.

trend of blue shift matches better with larger chip size. For smaller chip size such as 25 and 10  $\mu\text{m}$ , the trend is slightly different. The discrepancy may be due to several possible reasons: (1) the current crowding effect is different for different chip sizes. Hence, the red shift may not occur for different current densities in the QW as predicted by 1D simulations; (2) for the high indium QW, a large random alloy fluctuation or indium segregation is expected. Hence, the filling of states may not be the same as the ideal cases; (3) although the compressive InGaN is relaxed to 0.38 GPa<sup>12</sup>, the top multi-QWs of InGaN still suffer from compressive strain. Hence, the wavelength shift results from a combination of the screening of QCSE, quantum effect, and band filling. This is a complex phenomenon and requires further study. By contrast, there exist extra emission spectra at 380 and 450 nm for the smallest  $\mu$ -LEDs for high injection current density, as shown in Fig. 3b. Obviously, the overflow current and band filling phenomena occur in the red InGaN  $\mu$ -LEDs. The inset of Fig. 3b also shows the emission images of the  $10 \times 10 \mu\text{m}^2$   $\mu$ -LED injected at the current from 0.1 to 10 mA. In the simulation, if the leakage path is strong in the epilayer, with a higher density of tail states in the simulation, we also observe that some holes will reach the blue QWs for current density larger than  $10^3 \text{ A/cm}^2$  and an emission of blue QWs will be observed. These leakage paths may come from dislocation line and Vpits<sup>12</sup>.

## Conclusion

In this study, five InGaN red light  $\mu$ -LEDs with areas  $100 \times 100$ ,  $75 \times 75$ ,  $50 \times 50$ ,  $25 \times 25$ , and  $10 \times 10 \mu\text{m}^2$  were successfully produced. The leakage current density increases as the size decreases under a reverse voltage less than 3 V. As the reverse voltage increases ( $> 3 \text{ V}$ ), the leakage increases more obviously for larger chip size, especially for the  $\mu$ -LED with  $100 \times 100 \mu\text{m}^2$ . This suggests that not only is the leakage current relative to the sidewall passivation and the lateral electric field, the defects distributed on the surface could also affect the leakage current density. The optical output power increases for all the chips with the injected current. When the injection current was 0.1 mA, the emission wavelengths of  $\mu$ -LEDs from large to small were 663.78, 651.76, 645.51, 639.97, and

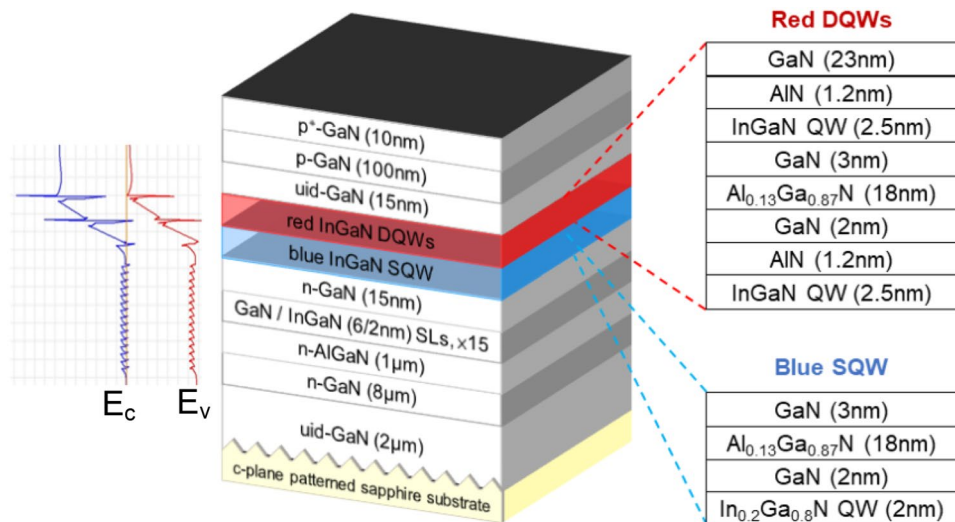


**Figure 4.** Schematic diagram of red InGaN  $\mu$ -LED epitaxial structure and the corresponding energy bandgap.

617.15 nm. As the size of the  $\mu$ -LED decreased, the injection current of the small-sized  $\mu$ -LED increased, the blue shift of the emission wavelength caused by the band filling effect became more obvious. In order to maintain the red color emission (wavelength > 615 nm) for the  $10 \times 10 \mu\text{m}^2$ , it should be operated current less than 100  $\mu\text{A}$ . The results indicate that InGaN materials can successfully produce red  $\mu$ -LEDs with a minimum size of  $10 \times 10 \mu\text{m}^2$ , which has the potential to become a full-color display of InGaN structure with blue and green light for  $\mu$ -LEDs display applications.

## Experimental

The red InGaN  $\mu$ -LED structure was grown on the c-plane patterned sapphire substrate by MOCVD. First, an undoped thick GaN layer with 2  $\mu\text{m}$  thickness was grown to reduce the residual stress and improve the quality of the following InGaN quantum well (QW). Then, the Si-doped n-type GaN layer with 8  $\mu\text{m}$  thickness and 15 pairs of GaN(6 nm)/InGaN(2 nm) superlattice layers were grown for stress engineering. Subsequently, a blue InGaN single-layer QW with a small amount of In and 2 pairs of red InGaN QWs with a large amount of In, and p-type GaN doped with Mg were sequentially grown. Figure 4 shows the details of the epitaxial layer structure as well as the band diagram. The crystal properties and microstructure examined by atomic force microscopy, scanning electron microscope and transmission electron microscope have been studied and published<sup>12</sup>. After, the epilayer was cleaned by acetone, isopropanol, and deionized water, an indium tin oxide (ITO) film with 280 nm thickness was deposited on p-GaN using an electron gun evaporation system as the current spread layer. The samples were annealed at 525  $^{\circ}\text{C}$  for 20 min to make the ITO and the p-type GaN layer present Ohmic contact.

In this study, laser direct writing (Heidelberg Instruments, MLA-150) exposure technology was used for the pattern process without mask, and  $\mu$ -LEDs of different sizes (i.e.,  $100 \times 100$ ,  $75 \times 75$ ,  $50 \times 50$ ,  $25 \times 25$ , and  $10 \times 10 \mu\text{m}^2$ ) were fabricated on the same epitaxial wafer. After the mesa pattern, the epilayer was etched to the n-GaN layer by an inductively coupled plasma reactive ion etching (ICP-RIE) system. Then, Ti/Al/Ti/Au/Cr multilayer metals were deposited on the n-GaN as the n-contact electrode, and 525-nm-thick  $\text{SiO}_2$  was grown by plasma enhanced chemical vapor deposition (PECVD) as the passivation layer to repair the dry etching damage on the sidewalls of the  $\mu$ -LEDs and the insulating layer to isolate the anode and cathode metal electrodes. Finally, Cr/Al/Ti/Au multilayer metals with a thickness of approximately 1  $\mu\text{m}$  were deposited as the p contact electrode by an electron gun evaporation system. Details on the fabrication flowchart of  $\mu$ -LEDs are shown in Fig. 5a. It is important to mention that the p-electrode contact pads for all sizes were extended to the mesa area for easy measurement. All the p-electrode dimensions are shown in Fig. 5b; they cover about 15% of the emission area.

After processing, the current–voltage ( $I$ – $V$ ) and output power characteristics of these  $\mu$ LEDs were measured at room temperature. The EQE was obtained by on-wafer measurements which the integrating sphere covers the wafer and light was collected through the surface, shown in the inset of Fig. 2b. Due to the limited collection angle and lack of light extraction enhancements (without encapsulation by epoxy), the measured EQE values could be lower compared to values obtained if the devices were encapsulated and the total extracted light collected in an integrating sphere. Even though, the EQE was calibrated using a TO-Can packaged red GaInN LED with  $300 \mu\text{m} \times 300 \mu\text{m}$  (with the same fabrication process and epilayer) without encapsulated by epoxy and was measured in an integrating sphere. All data were averaged using 20  $\mu$ LEDs devices.

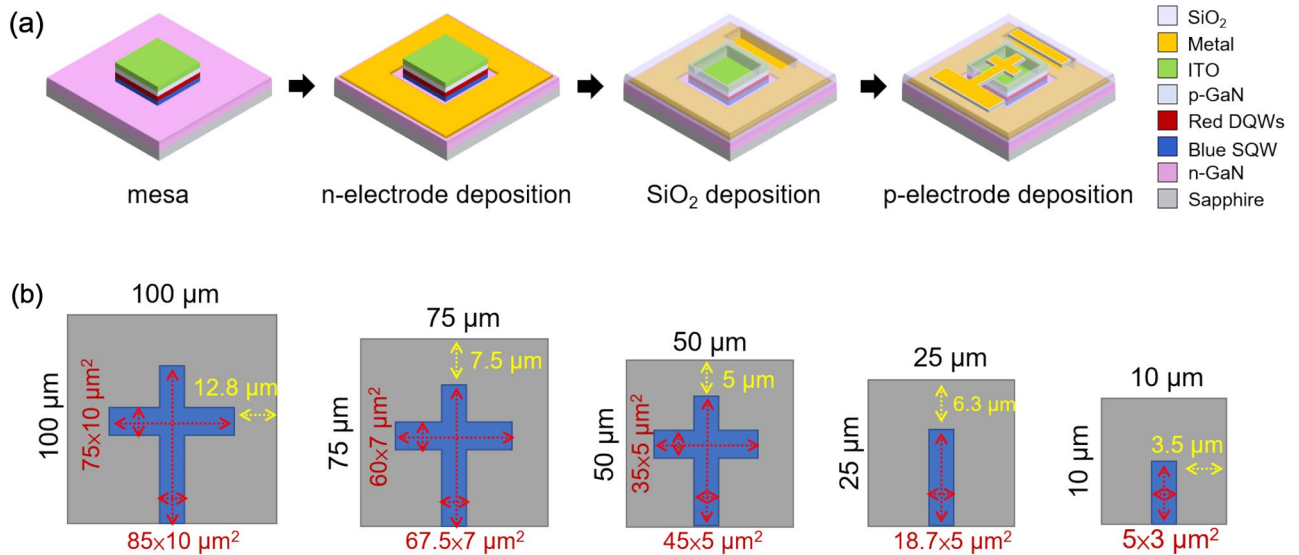


**Figure 5.** (a) Fabrication flowchart of  $\mu$ -LEDs and (b) all the p-electrode dimensions of  $\mu$ LEDs.

Received: 12 October 2021; Accepted: 3 January 2022

Published online: 25 January 2022

## References

- Huang, Y., Hsiang, E. L., Deng, M. Y. & Wu, S. T. Mini-LED, micro-LED and OLED displays: Present status and future perspectives. *Light Sci. Appl.* **9**(1), 1–16 (2020).
- Lin, J. Y. & Jiang, H. X. Development of microLED. *Appl. Phys. Lett.* **116**(10), 100502 (2020).
- Tian, P. *et al.* Size-dependent efficiency and efficiency droop of blue InGaN micro-light emitting diodes. *Appl. Phys. Lett.* **101**(23), 231110 (2012).
- Olivier, F. *et al.* Influence of size-reduction on the performances of GaN-based micro-LEDs for display application. *J. Lumin.* **191**, 112–116 (2017).
- Kou, J. *et al.* Impact of the surface recombination on InGaN/GaN-based blue micro-light emitting diodes. *Opt. Express* **27**(12), A643–A653 (2019).
- Takeuchi, T. *et al.* Quantum-confined Stark effect due to piezoelectric fields in GaInN strained quantum wells. *J. Appl. Phys.* **36**(4A), L382 (1997).
- Han, S. *et al.* AlGaInP-based micro-LED array with enhanced optoelectrical properties. *Opt. Mater.* **114**, 110860 (2021).
- Wong, M. S. *et al.* Improved performance of AlGaInP red micro-light-emitting diodes with sidewall treatments. *Opt. Express* **28**(4), 5787–5793 (2020).
- Iida, D., Zhuang, Z., Kirilenko, P., Velazquez-Rizo, M. & Ohkawa, K. Demonstration of low forward voltage InGaN-based red LEDs. *Appl. Phys. Express* **13**(3), 031001 (2020).
- Hwang, J. I., Hashimoto, R., Saito, S. & Nunoue, S. Development of InGaN-based red LED grown on (0001) polar surface. *Appl. Phys. Express* **7**(7), 071003 (2014).
- Zhang, S. *et al.* Efficient emission of InGaN-based light-emitting diodes: Toward orange and red. *Photonics Res.* **8**(11), 1671–1675 (2020).
- Iida, D. *et al.* 633-nm InGaN-based red LEDs grown on thick underlying GaN layers with reduced in-plane residual stress. *Appl. Phys. Lett.* **116**(16), 162101 (2020).
- Iida, D., Niwa, K., Kamiyama, S. & Ohkawa, K. Demonstration of InGaN-based orange LEDs with hybrid multiple-quantum-wells structure. *Appl. Phys. Express* **9**(11), 111003 (2016).
- Pasayat, S. S. *et al.* Demonstration of ultra-small (< 10  $\mu\text{m}$ ) 632 nm red InGaN micro-LEDs with useful on-wafer external quantum efficiency (> 0.2%) for mini-displays. *Appl. Phys. Express* **14**(1), 011004 (2020).
- Iida, D. *et al.* Enhanced light output power of InGaN-based amber LEDs by strain-compensating AlN/AlGaIn barriers. *J. Cryst. Growth* **448**, 105–108 (2016).
- Oh, J. T. *et al.* Light output performance of red AlGaInP-based light emitting diodes with different chip geometries and structures. *Opt. Express* **26**(9), 11194–11200 (2018).
- Piprek, J. Efficiency droop in nitride-based light-emitting diodes. *Phys. Status Solidi A* **207**(10), 2217–2225 (2010).
- Zhuang, Z., Iida, D. & Ohkawa, K. Investigation of InGaN-based red/green micro-light-emitting diodes. *Opt. Lett.* **46**(8), 1912–1915 (2021).
- Wu, Y. R. One dimensional Drift-diffusion charge control solver (1D-DDCC). <http://yrwu-wk.ee.ntu.edu.tw/>
- Li, C. K. *et al.* 3D numerical modeling of the carrier transport and radiative efficiency for InGaN/GaN light emitting diodes with V-shaped pits. *AIP Adv.* **6**(5), 055208 (2016).

## Acknowledgements

This work was supported by the Ministry of Science and Technology, Taiwan, under Grant Nos. MOST 110-2218-E-A49-012-MBK, 110-2622-8-009-018-SB, 109-2224-E-009-002, 109-2221-E-009-143-MY3, 109-2634-F-009-028, 108-2628-E-002-010-MY3, 108-2622-E-009-009-CC2, 108-2618-E-009-031. We would like to thank Taiwan Semiconductor Research Institute for processing supporting.

### Author contributions

The manuscript was completed through the contributions of all authors. R.H.H. conceived the idea, contributed to the data analyses and prepared the manuscript. C.X.Y. fabricated the devices. P.W.C. and D.S.W. contributed to uLED characteristics measurement. D.I. and K.O. contributed to the red GaInN LED epilayer growth.

### Competing interests

The authors declare no competing interests.

### Additional information

**Correspondence** and requests for materials should be addressed to R.-H.H. or D.-S.W.

**Reprints and permissions information** is available at [www.nature.com/reprints](http://www.nature.com/reprints).

**Publisher's note** Springer Nature remains neutral with regard to jurisdictional claims in published maps and institutional affiliations.



**Open Access** This article is licensed under a Creative Commons Attribution 4.0 International License, which permits use, sharing, adaptation, distribution and reproduction in any medium or format, as long as you give appropriate credit to the original author(s) and the source, provide a link to the Creative Commons licence, and indicate if changes were made. The images or other third party material in this article are included in the article's Creative Commons licence, unless indicated otherwise in a credit line to the material. If material is not included in the article's Creative Commons licence and your intended use is not permitted by statutory regulation or exceeds the permitted use, you will need to obtain permission directly from the copyright holder. To view a copy of this licence, visit <http://creativecommons.org/licenses/by/4.0/>.

© The Author(s) 2022